PERGAMON

Journal of Structural Geology 23 (2001) 297–313

JOURNAL OF STRUCTURAL GEOLOGY

www.elsevier.nl/locate/jstrugeo

Geometry and distribution of regional joint sets in a non-homogeneous stress field: case study in the Ebro basin (Spain)

L. Arlegui[a,b,*], J.L. Simón[a]

[a]*Departamento de Geología, Universidad de Zaragoza, 50009 Zaragoza, Spain*
[b]*Laboratory for Strain Analysis, Department of Earth Sciences, Cardiff University, Cardiff CF1 3YE, UK*

Received 12 November 1999; accepted 29 June 2000

Abstract

Three regional joint sets striking N–S, E–W and WNW–ESE affect the Tertiary rocks of the central Ebro basin. From analysis of their chronological relationships and spatial distribution, it is concluded that they correspond to two different tectonic events. The N–S set (oldest) and the E–W set (younger) are present in the southern and central sectors, while the WNW–ESE joint set predominates in the northern one. The N–S joints propagated in response to joint-normal and fluid loads under an intraplate stress field with S_{Hmax} oriented near N–S (related to forces caused by the convergence of Africa, Iberia and Europe and rifting at the Valencia trough) during the sedimentary infilling of the basin. These joints are only present in the southern part of the area. The E–W joint set in the southern-central sector records the same fracturing event as the WNW–ESE set does in the northern one. Its orientation was modified by the presence of the older N–S set in the south, which perturbed the regional stress field. The younger WNW–ESE and E–W joint sets are interpreted as unloading joints. These propagated as a consequence of flexural uplift and exhumation related to isostatic rebound at the Pyrenees and the Ebro foreland basin. A numerical approach is used to explain the inhomogeneous distribution of the N–S joint set in terms of their absence being controlled by the depth of the water table at the time of their formation.

1. Introduction

1.1. Scope of the work

Joint sets are characterised by consistency of orientation over wide areas. As a result, they have been extensively used to map regional stress trajectories (Engelder and Geiser, 1980; Holts and Foote, 1981; Hancock, 1985; Bevan and Hancock, 1986; Simón, 1989; Hancock and Engelder, 1989; Liotta, 1990; Bergerat et al., 1991; Hancock, 1991; Arlegui and Simón, 1993; Arlegui 1996). One of the main reasons to map paleostress orientations from joints is their systematic development. Joints are sensitive markers of small stress changes, and curving joints reflect inhomogeneous stress fields (Pollard et al., 1982; Rawnsley et al., 1992). Also, they occur pervasively in shallow tectonic environments, especially in relatively undeformed basins and platforms. In such cases they are quite often the only available structure for mapping the orientation of paleostress.

Joints are used as indicators of paleostress orientations because they form normal to σ_3 and parallel to the $\sigma_1\sigma_2$ plane (Griffith, 1920, 1924; Price, 1966; Pollard and Aydin, 1988). When several joint sets co-exist in one site, geometrical and chronological relationships supply information about fracture development and paleostress evolution. By compiling results from a large number of outcrops, paleostress fields may be reconstructed.

The Ebro basin, in the Spanish Pyrenean foreland (Fig. 1), is a region where joints are especially useful for mapping paleostress. Regional stress fields changed in space and time as collision progressed during the Neogene (Simón, 1989; Arlegui, 1996; Cortés, 1999; Simón et al., 1999; Liesa, 2000). Macrostructural evidence for the paleostress changes is poor, but joints are abundant and should provide a reliable picture of paleostress fields. In this paper, we describe the joint patterns in the Ebro and propose a dynamic model to attempt to explain Neogene paleostress evolution within the northeastern Iberian Peninsula. Paul Hancock (Hancock and Engelder, 1989; Turner and Hancock, 1990; Hancock, 1991; Arlegui and Hancock, 1991) pioneered the studies of joints in the Ebro basin. He described several regional sets and detected some "enigmatic variations in neotectonic joint development" (Hancock, 1991), which are the focus of the present work.

* Corresponding author. Tel.: 00-34-976-76-21-26; fax: 00-34-976-76-10-88.
E-mail address: arlegui@posta.unizar.es (L. Arlegui).

0191-8141/01/$ - see front matter
PII: S0191-8141(00)00097-3

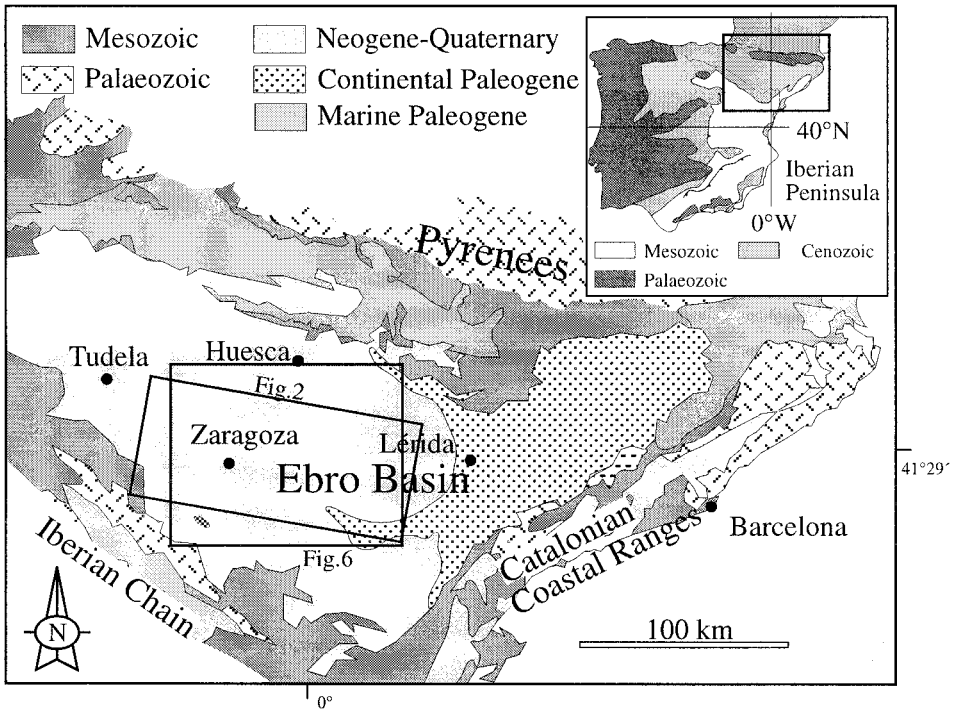

Fig. 1. Geological map of the NE Iberian Peninsula showing the location of the study area (Fig. 2).

1.2. Methodology

Not all joints in a structural domain may be examined. Thus, standard practice (Davis, 1984, p. 342) is to evaluate jointing through detailed analysis at selected sites. A total of 290 high-quality outcrops were studied in this work, where orientation and geometrical data about joints were collected. Data sites are located across the central Ebro basin, in both carbonate and clastic sedimentary rocks with ages ranging from late Oligocene to late Miocene. They typically consist of one or more near flat-lying beds of hard rock (either limestone or sandstone) with thickness ranging from 0.1 to 0.5 m, exposed at man-made cross-sections or small natural cliffs in the otherwise smooth slopes. In general, we followed scanlines along the exposures in which every single joint or fracture cutting the entire bed was measured and classified, till a minimum number of 50–60 measurements was accomplished. This number was recommended by Arlegui (1996) after analysing the stability of the mean and standard deviation of strike distributions from joint samples of different sizes.

The distribution of joint azimuths measured in each outcrop allows the definition of local joint sets. Both histograms and smoothed frequency curves (constructed following the *running average* technique: Wise and McCrory, 1982; Goldstein and Marshak, 1988) were used for this purpose. These curves enable a better determination of the mode of each set, in the same way as density diagrams allow a more accurate definition of maxima on equal-area stereoplots. Also, the mean and standard deviation were determined from the raw data, to avoid the influence of the smoothing procedure.

A number of criteria are used to determine the relative age of joint sets in given outcrops. Most are based on the fact that joints abut against previous fractures: direct abutting relationships, differential fracture length, forking and hooking structures in secondary fractures (Kulander et al., 1979; Hancock, 1985; Price and Cosgrove, 1990; Rives, 1992, Rawnsley et al., 1992; Arlegui, 1996). We carefully recorded geometrical and chronological relationships at every joint site. Some pavement surfaces, exposed at the bottom of dry gullies, provided high quality observations. We designed a portable telescopic tripod able to hang a camera up to 9 m high to obtain vertical photographs of them. Photomosaics were processed with image analysis techniques to yield detailed fracture maps.

Joint spacing was measured in 63 data sites. About 30 measurements were collected at each outcrop, following the same scanlines used for measuring joint azimuths. We measured spacing as the perpendicular distance between two neighbouring joints of the same set. As the structural literature points out, joint spacing usually increases with the thickness of sedimentary layers in a systematic fashion (Hobbs, 1967; Gross et al., 1995; Wu and Pollard, 1995). The ratio of mechanical layer thickness to median joint spacing for an individual layer is defined as the *fracture spacing ratio*, FSR (Gross, 1993). The slope of the best-fit line on a plot of both variables for a number of layers is the *fracture spacing index*, FSI (Narr and Suppe, 1991).

Development of a joint set has been described as a

process of *sequential infilling* (Gross, 1993). As the remote strain increases, spacing decreases by joints nucleating and propagating between early formed fractures. Eventually, fracture spacing stops evolving and remains nearly constant even with increasing strain. As this *saturation* state is achieved (Cobbold, 1979; Rives et al., 1992; Wu and Pollard, 1995; Gross et al., 1995), joints will have a strong modal spacing. We attempt to recognise the saturation degree through the use of two indices:

I_R = mode of spacing/mean spacing (Rives et al., 1992);
JPI = standard deviation of spacing/mean spacing (Dunne and Hancock, 1994).

JPI is an indicator of the regularity of joint spacing, whereas I_R is related to the symmetry of the spacing frequency distribution. According to the authors, when a contained joint set in a bed approaches saturation during formation, JPI tends to 0 and I_R tends to 1.

We studied the regional variation of these spacing indices by applying the *kriging* method. Kriging is a geostatistical gridding procedure based upon the concept of *regionalised variables* (Matheron, 1971; Watson, 1971) that generates contour and maps from irregularly distributed data points. It attempts to express trends that are suggested in the data set by fitting them to a mathematical model (*variogram model*). The latter mathematically specifies the spatial variability of the data set and determinates the interpolation weights applied to data points during the grid node calculations.

2. Regional framework

2.1. Geological setting of the Ebro basin

The Tertiary Ebro basin is bounded by three mountain ranges, the Pyrenees, the Iberian Chain and the Catalonian Coastal Ranges (Fig. 1), which controlled basin evolution (Riba et al., 1983; Cabrera, 1983; Puigdefàbregas and Souquet, 1986; Desegaulx and Moretti, 1988). Nevertheless, the Ebro basin mainly evolved as the southern foreland basin of the Pyrenees, developing a quite asymmetric shape. The depth of the Mesozoic–Tertiary boundary increases northward, reaching values of 4000 m below sea level under the southern Pyrenean thrust front (Riba et al., 1983). The Tertiary stratigraphic units also increase their thickness northward. This geometry is interpreted to be a consequence of subduction of the Iberian lithosphere beneath Europe. During the Palaeogene compression, the tectonic load of the Pyrenean allochthonous units and the formation of a cold lithospheric root (Brunet, 1986) is interpreted to have induced asymmetrical flexural subsidence of the Ebro basin (ECORS-Pyrenees Team, 1988; Roure *et al.*, 1989; Muñoz, 1992). By the late Miocene, some 10–15 m.y. after shortening decayed, isostatic rebound initiated, giving rise to the present-day elevated topography of the Pyrenees and inducing displacement on large-scale basement fractures under the Tertiary Ebro basin.

On the other hand, after the beginning of the Miocene, the convergence between Europe and Africa transferred to the southern margin of Iberia. The Ebro basin became an intraplate region subject to stress fields mainly related to the Africa–Iberia–Europe convergence and the extensional evolution of the Valencia Trough (Simón, 1989).

Most rocks exposed within the central Ebro basin are fluvial and lacustrine clastic, evaporite and carbonate facies deposited within an endorheic basin (Quirantes, 1978; Riba et al., 1983; Cabrera, 1983; Arenas, 1993; Arenas and Pardo, 1994). Their ages range from late Oligocene to early late Miocene (Vallesian). Oligocene deposits are synorogenic, whereas Miocene deposits are essentially post-orogenic.

2.2. Macrostructure of the central Ebro basin: geometry and kinematics

The shallow structure of the central Ebro basin is defined by the Ebro syncline (Quirantes, 1978; Arlegui, 1996), a WNW–ESE-trending fold with a length exceeding 200 km and gently dipping limbs (Fig. 2a). A dense ensemble of lineaments identified on aerial photographs and satellite images (Arlegui et al., 1994, Arlegui and Soriano, 1998) occupy the core of this syncline. The dominant set trends WNW–ESE and shows its maximum density between the southern slopes of the Alcubierre range and the Ebro River (Fig. 2b). Field observations and seismic reflection data indicate that these lineaments mainly correspond to normal faults with metre-scale offsets.

At depth, seismic and well information compiled by Lanaja (1987) and IGME (1990) allow us to interpret structural patterns parallel to the Ebro syncline (see Fig. 2c). Briefly, some ESE striking faults were inferred from the contour map of the top of the middle Triassic (Lanaja, 1987, map 3). At the same time, isopachs of the upper Triassic show a trough located immediately to the north of the syncline hinge, where the thickness of the upper Triassic reaches four times its regional standard thickness (IGME, 1990, map 164).

A cross-section was constructed using this information plus recent geological maps (ITGE, 1995a,b), well data (Lanaja, 1987) and some unpublished seismic reflection data (Fig. 3). The Ebro syncline folds the Miocene units, whereas its amplitude decreases downward into Oligocene rocks and it vanishes in the Eocene rocks, which both thicken to the NNE. We interpret the faults appearing in the middle Triassic and the anomalous thickness of the upper Triassic detachment level as related to a basement normal fault, whereas cover deformation was accommodated by the Ebro syncline.

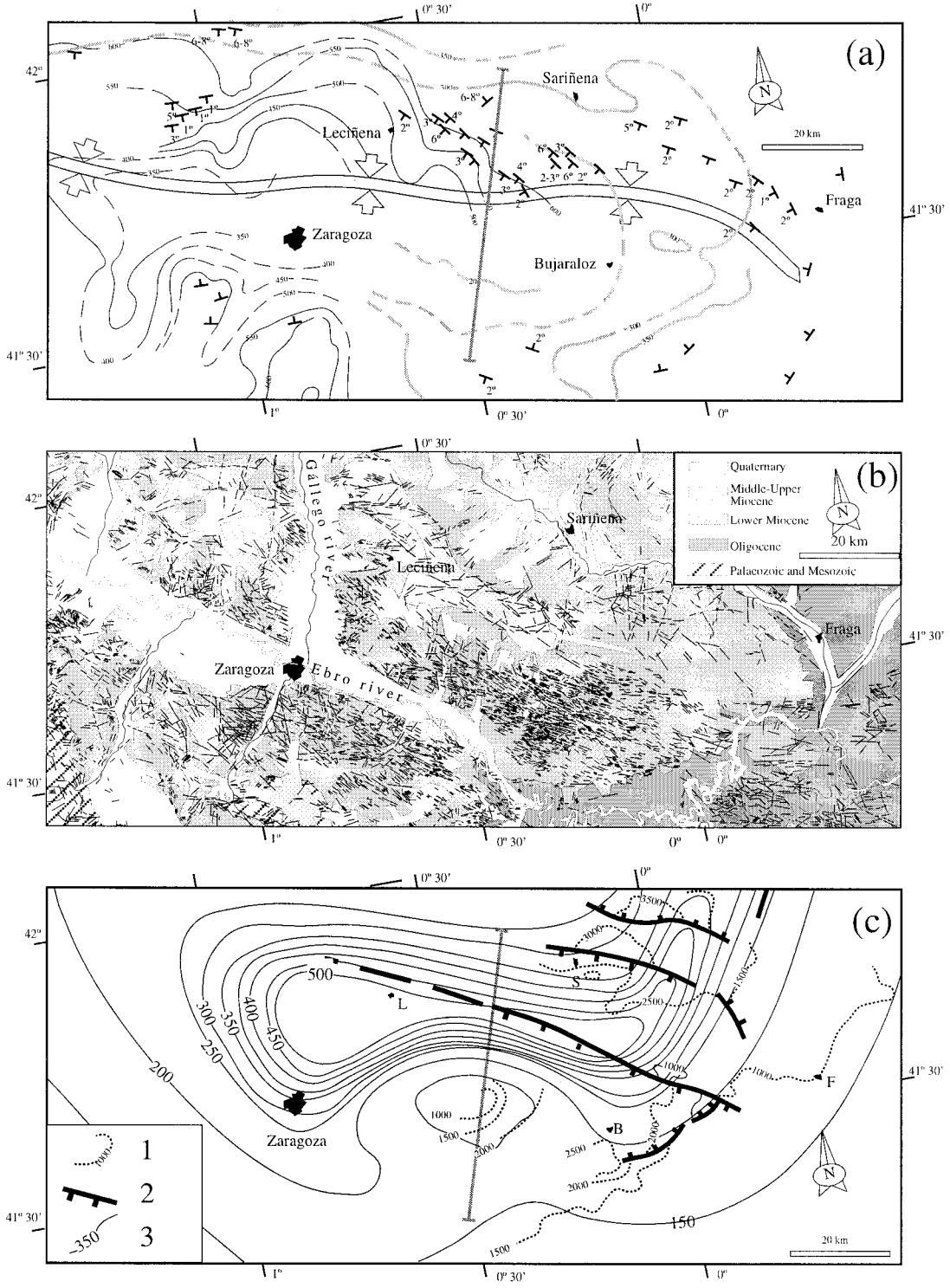

Fig. 2. (a) Contour map of the boundary between Bujaraloz-Sariñena and Remolinos-Lanaja Formations (lower Aragonian, lower Miocene), in black, and the boundary between Pallaruelo-Monte de la Sora and Montes de Castejón Formations (middle-upper Aragonian), in grey. Bedding measurements with dip amounts and the trace of the Ebro syncline are also displayed. (b) Lineaments in the central Ebro Basin (after Arlegui and Soriano, 1998). (c) Overview of the structure at depth. (1) Contours of top of the middle Triassic (modified from Lanaja, 1987). (2) Major faults in the basement inferred from the former contours. (3) Isopachs of the upper Triassic (modified from IGME, 1990). The straight grey line in (a) and (c) indicates location of the cross-section of Fig. 3.

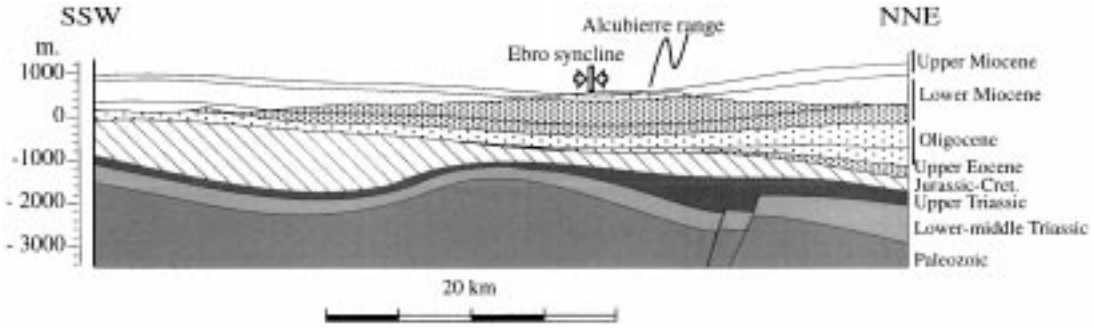

Fig. 3. Cross-section through the central part of the study area (see location in Fig. 2a, c).

3. Description of joints

3.1. Definition of regional joint sets

As joints in this area are usually vertical, their orientation was described by azimuth only, and local sets were defined using azimuth histograms and smoothed frequency curves (Fig. 4). Some stations show a systematic (continuous, planar, parallel, evenly spaced) N–S joint set accompanied by secondary (younger) E–W cross joints abutting the former (mean azimuths 004 ± 7°and 092 ± 10°, respectively, in the example of Fig. 4a). Other sites show a primary (older) WNW–ESE set with NNE–SSW cross joints (mean azimuths 115 ± 10° and 027 ± 12° in the example of Fig. 4b). Both types of joint patterns are illustrated in Fig. 4c, d.

After carrying out the analysis of the 290 field sites,

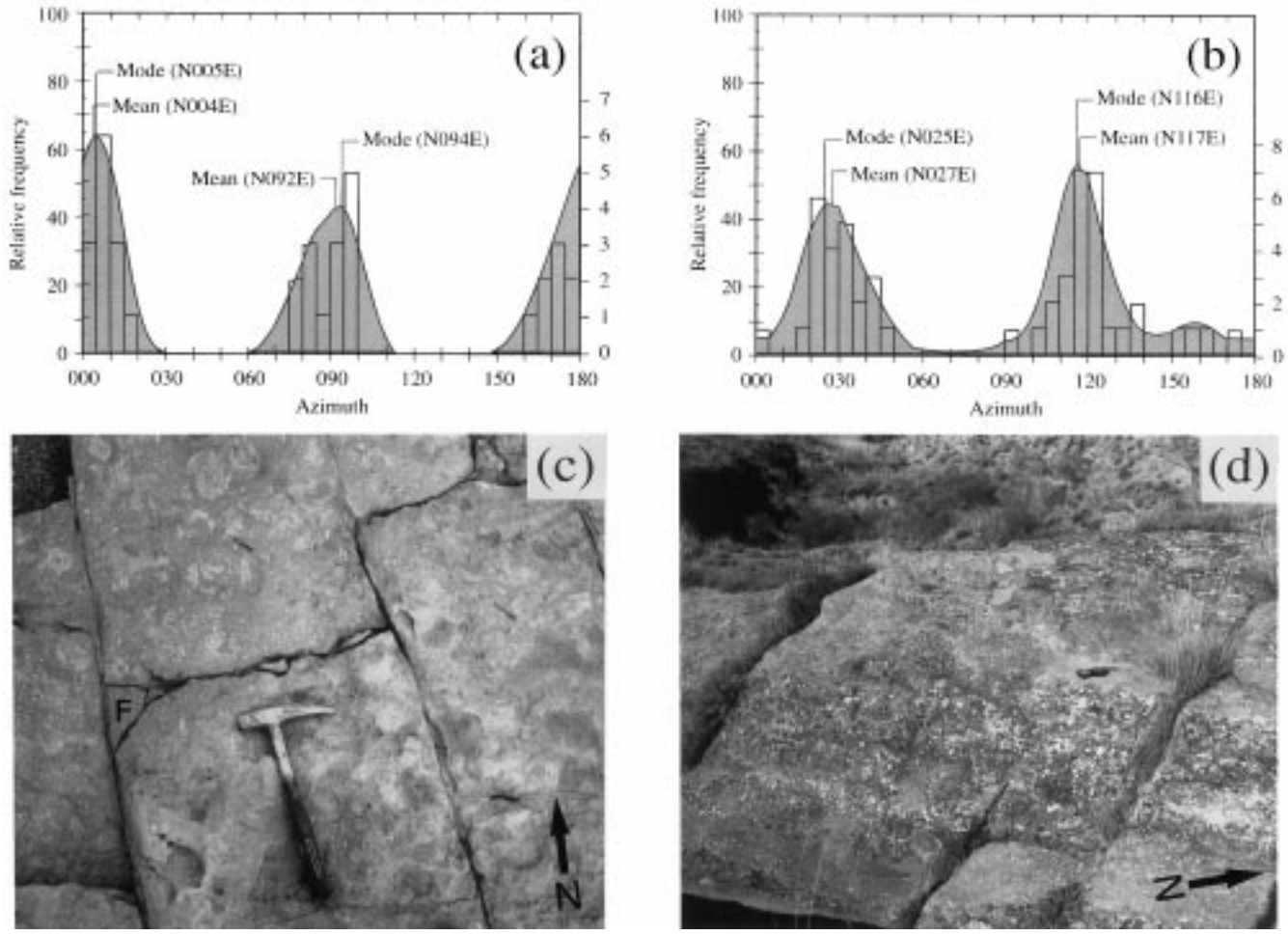

Fig. 4. Joint sets at individual sites. (a) Histogram and smoothed frequency curve showing well-developed N–S and E–W joint sets; site 1 in Fig. 6. (b) Dominant WNW–ESE joint set with NNE–SSW cross joints; site 2 in Fig. 6. (c) Field aspect of joint geometry similar to (a), showing E–W younger cross joints abutting older N–S ones; F: forking structures; site located near Tudela (see Fig. 1). (d) Field aspect of joint geometry similar to (b); site 3 in Fig. 6.

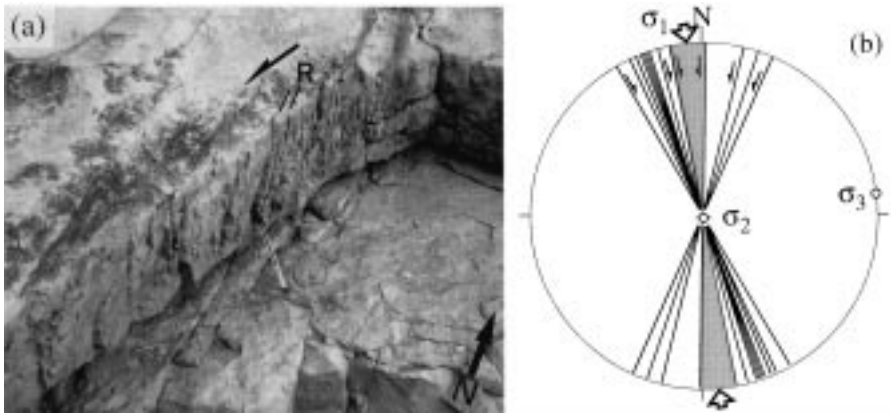

Fig. 5. Shear fractures at site 4 (see location in Fig. 6). (a) Shear (left lateral) fracture showing en échelon Riedel minor fractures (R) with no observed offset. (b) Orientation of conjugate shear planes compatible with a horizontal, 175°-trending σ_1 axis.

which involves processing more than 13,000 azimuth data, some features may be generalised at a regional scale. First, their azimuth distributions show a number of persistent maxima. The three main joint sets found in examples of Fig. 4 (N–S, E–W and NW–SE) are the most important and pervasive. Each one is characterised by its mean azimuth, deviation, spacing distribution and time relationships with respect to other structures. In summary, they all may be considered as well-defined *regional joint sets* whose main characteristics are described next.

The *N–S joint set* (NNW striking joints of Hancock and Engelder, 1989, and Hancock, 1991) comprises well-developed, systematic joints: planar, parallel with regular, bed-thickness-dependent spacing. The average strike of this set is 176 ± 11°. Their traces on bedding are persistent and typically have lengths of several metres to several tens of metres. Vertical continuity is usually limited to bed thickness.

The *E–W joint set* is composed of short joints whose horizontal length is limited by spacing of the N–S joint set (Fig. 4c). Both sets typically compose a cross joint geometry (Hodgson, 1961) or H-shaped pattern (Hancock, 1985). The average orientation is 087 ± 8°. Joint surfaces are not so planar as the N–S joints, and spacing is wider than the former. Given their cross joint geometry, they should be considered as non-systematic, according to Hodgson (1961). Nevertheless, they are quite regular in form, spacing and orientation (in fact, on average they show smaller standard deviation than the N–S set: 8° vs. 11°).

WNW–ESE joint set. The average strike of this set is 110 ± 21° (less persistent in orientation than the other sets). Their bed-parallel trace length may attain several tens of metres, and they show a quite regular, bed-thickness-dependent spacing. They are often accompanied by roughly orthogonal, completely irregular cross joints (Fig. 4d).

The E–W and WNW–ESE joint sets show quite similar ranges of modal directions (060–120° and 070–150°, respectively), but they differ in architectural style. In general, N–S and WNW–ESE joints are persistent parallel joints that are older than other fractures in their host rocks, whereas E–W joints are younger cross joints found with N–S ones (Fig. 4c, d). The presence of hooks and forking structures corroborates this timing relationship. N–S joints acted as mechanical layer boundaries controlling length and spacing of E–W joints (Fig. 4c) like bedding surfaces (Gross, 1993; Ruf et al., 1998).

Joints of every set are interpreted as Mode I fractures. Many N–S and E–W joint surfaces are quite smooth or exhibit well-developed hackle marks and gentle ribs. This ornamentation has not been observed on NW–SE joints but, on the other hand, neither do these show any shear indicators. A number of surfaces nearly parallel to N–S joints have small, closely spaced en échelon Riedel fractures (Fig. 5a). These fractures have been interpreted as conjugate strike-slip shear fractures without noticeable displacement (Hancock and Engelder, 1989; Simón et al., 1999). More precisely, fractures striking N to NNE show left-lateral shear, whereas those striking N to NNW show right-lateral shear (Fig. 5b). In this way, N–S Mode I and both types of shear fractures are compatible with the same stress axes: N–S-trending σ_1 and E–W-trending σ_3.

3.2. Spatial distribution and time relationships of the primary joint sets

The two systematic regional joint sets, N–S and WNW–ESE, are not distributed homogeneously across the central Ebro basin (Fig. 6). Hancock (1991) also observed this heterogeneity and defined a domain of systematic WNW–ESE joints extending along the northern fringe of the Ebro basin. In contrast, the N–S set occupies the southern sector, between the Alcubierre-Sigena ranges and the Iberian Chain. The map trace of the boundary between both joint domains is marked as a dotted line in Fig. 6.

A number of observations indicate that the domain of N–S joints is not only *southward*, but also locally *upward*, with respect to the WNW–ESE joint domain. The map trace of

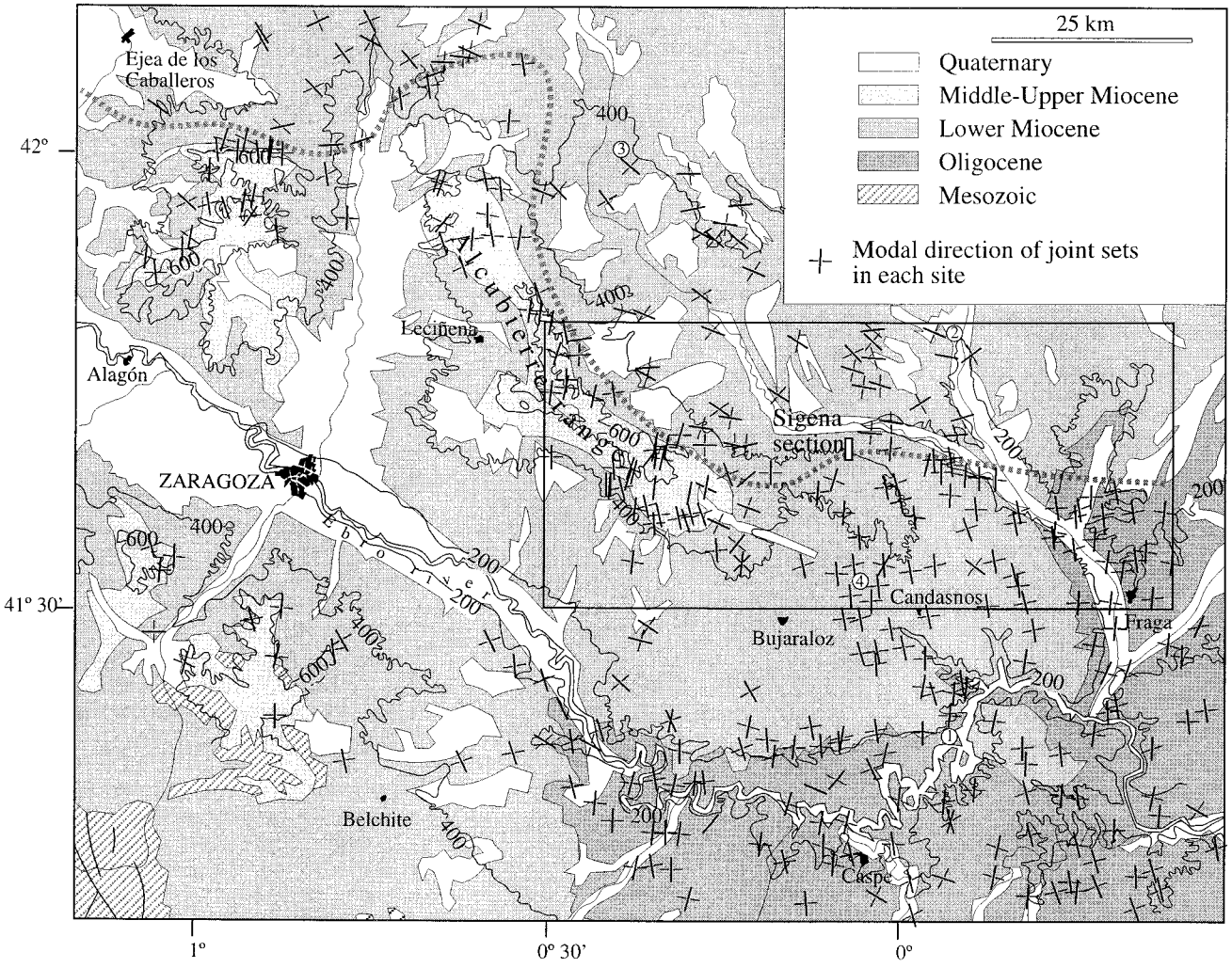

Fig. 6. Modal direction of joint sets at each data site. Continuous line: primary (older) set; broken line: secondary (younger) set. The area represented in Fig. 10 is marked as a rectangle. The dotted line represents the boundary between the N–S and the WNW–ESE systematic joint domains. Small numbers indicate data sites shown in Figs. 4 and 5. Height contours in metres above sea level (m.a.s.l.).

the boundary in the northern side of the Alcubierre-Sigena ranges (see Fig. 6) runs close to the lower/upper Miocene limit, and also close to the 500 m.a.s.l. contour line. The WNW–ESE and N–S joint sets occur, respectively, below and above that altitude. An example of the actual vertical distribution of joints in this zone was obtained from a detailed survey in a section across the northern slope of the Sigena range (see Fig. 7, location in Fig. 6). Both joint domains are clearly differentiated in that section, although they are found together within a narrow "joint transition zone" at altitudes between 460 and 490 m (Hancock, 1991; Arlegui, 1992, 1996).

This transition zone has been also recognised in other locations of the Alcubierre-Sigena ranges, and it is very interesting because cross-cutting relationships between the N–S and WNW–ESE joint sets can be observed there. These relationships indicate that the WNW–ESE joints consistently abut (so they are younger than) the N–S ones (Fig. 8).

3.3. Relationships between WNW–ESE and E–W joint sets

The former result poses the question of the exact nature of the WNW–ESE and E–W joint sets. Their strike ranges overlap, and both show identical timing relationships with respect to the N–S set. So, do they actually represent two independent joint sets? This question may also be investigated at the "transition zone" within the Sigena section, where all three joint sets are found together. Exhaustive observations in this zone indicate that:

E–W and WNW–ESE joints tend to develop in separate domains, so that cross-cut relationships between them are very scarce. The observed examples show that joints of both orientations abut each other, and some of them propagate in a curved path changing from WNW–ESE to E–W strike (Fig. 9a). These geometries suggest that both joint sets were coeval.

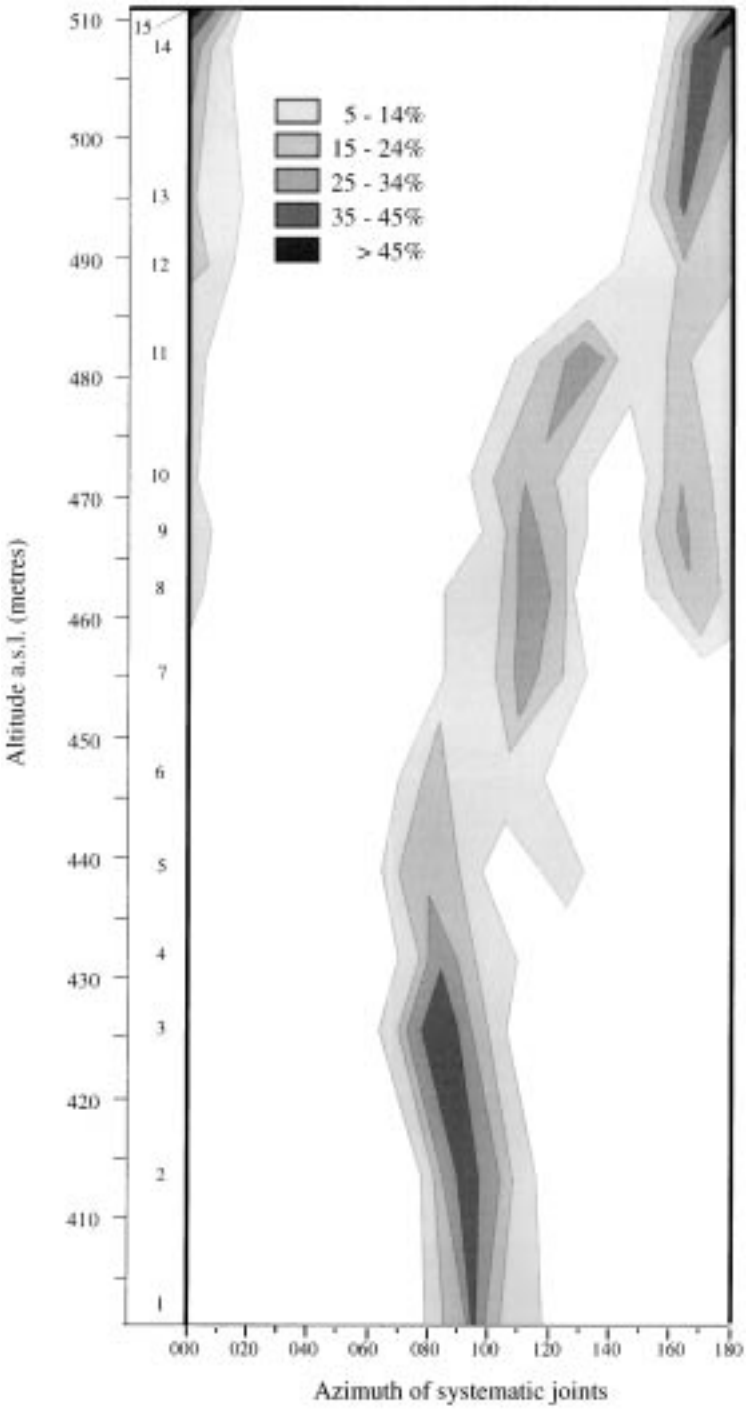

Fig. 7. Azimuth variation of systematic joints across the Sigena section (see location in Fig. 6). Numbers 1–15, on the left, indicate the location of individual data sites where detailed observations were made. Shading indicates the relative frequency of azimuths. In spite of their abutting relations with respect to the N–S set, WNW–ESE joints in the transition zone between 460 and 490 m.a.s.l. are also included.

The distribution of WNW–ESE and E–W joints has a strong dependence on spacing of the N–S ones: WNW–ESE joints are common between widely spaced N–S joint pairs, whereas E–W joints are found where the latter are closely spaced. Fig. 9b shows a plot of azimuths of secondary or younger joints (WNW–ESE to E–W) versus normalised spacing of the primary N–S joints for two limestone beds within the transition zone. Joints striking 060–090° (so orthogonal to the N–S systematic set, azimuth = 166 ± 8°) occur for spacing to layer thickness ratio below 0.8. Above this value, secondary joints tend to propagate according to the mean orientation of the WNW–ESE regional set (110°).

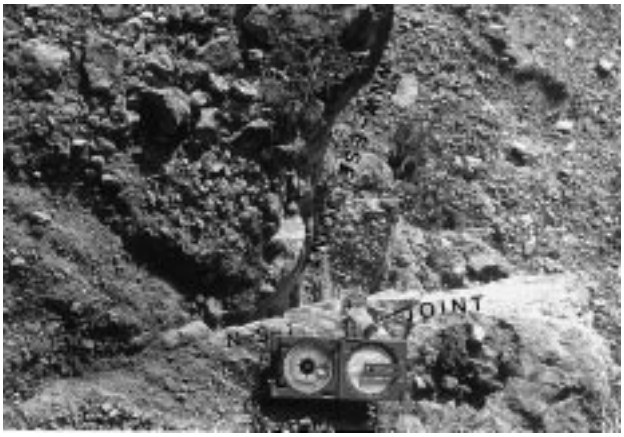

Fig. 8. Field example showing abutting relationships between joints oriented N–S (older) and WNW–ESE (younger) in the transition zone of the Sigena section (see location in Fig. 6).

These data allow us to construct a model of joint architecture that is represented schematically in Fig. 9c and can be easily identified in the actual field example shown in Fig. 9d. We apply the dynamic explanation proposed by Engelder and Gross (1993) for a similar case described in the Appalachian Plateau. According to this, we interpret that the secondary WNW–ESE and E–W joints in the "transition zone" of the Sigena section (and so the WNW–ESE and E–W regional joint sets) make up an only set. The occurrence of either one or another joint direction is related to stress perturbation phenomena induced by the N–S set. If N–S joints are close enough to each other, stress perturbation affects the whole volume between them and near planar cross joints develop normal to N–S shear-stress-free surfaces (Simón et al., 1988; Gross, 1993; Caputo, 1995). If N–S joints are further apart, WNW–ESE joints develop without interference or modification except at their tips, where curving perpendicular geometry may occur as a consequence of stress perturbation in the vicinity of N–S joint surfaces. According to Dyer (1988), this geometry requires a net far field tensile stress both normal and parallel to the pre-existing N–S joints.

3.4. Spacing variation of the N–S joint set

Spacing characteristics of the systematic N–S joint set change within its regional domain. Spacing data for these joints are available from 63 outcrops distributed across the central and eastern study area, close to the domain boundary of the Alcubierre-Sigena ranges (Fig. 10, see location in Fig. 6). The ratio of layer thickness to median spacing for the ensemble of stations is FSI = 1.20 (Fig. 10a). Mean values of indices I_R and JPI are 0.89 and 0.44, respectively. All these features indicate that, on average, the degree of saturation is medium to high.

Nevertheless, the dispersion of individual plots in Fig. 10a, as well as deviation of I_R and JPI values, are significant. This variation cannot be attributed to lithological variation since lithology is quite homogeneous (chalky limestone) in all the studied outcrops. On the contrary, deviation may be a consequence of differences in joint saturation degree. We explored this possibility by analysing the spatial variation of indices for spacing by means of the kriging technique. The results are plotted on three contour maps that show the regional variations of FSR, I_R and JPI indexes, respectively (Fig. 10b–d). The pattern of this variation is consistent for all the three maps, showing that saturation of the N–S joints decreases approximately from SSW toward NNE. This tendency is more evident for the FSR values, which have a more immediate relationship with the degree of saturation.

The overall spacing variation suggests that the change from the southern N–S joint domain to the northern WNW–ESE joint domain does not occur suddenly. The average saturation of the N–S joints gradually diminishes northward until the set becomes absent in most of the Miocene series to the north of the Alcubierre-Sigena ranges.

4. Discussion and interpretation

4.1. Genetic classification of joints: relationships to regional stress fields and macrostructures

The features of fracture sets described above may be summarised and interpreted as follows. First the joints measured in the region may be grouped into three sets, N–S, E–W and WNW–ESE, the N–S set being older than the E–W and WNW–ESE sets. The E–W and WNW–ESE sets are coeval and genetically related, as demonstrated at the transition zone of the Sigena section, where the three joint sets have been found together. Their only difference is that the WNW–ESE joints formed normal to the regional minimum horizontal stress, whereas E–W joints formed where the presence of N–S joints as free surfaces perturbed the stress field. Consequently, the presence of the N–S joints in the southern sector perturbed the local stress field and induced the development of new secondary E–W joints normal to them.

According to this, only two *genetic joint sets* related to two different stress fields and geodynamic mechanisms should be defined:

The *N–S joint set* developed under a stress field with S_{Hmax} oriented near N–S. Joints could be compatible with either $S_{Hmax} = \sigma_1$ or $S_{Hmax} = \sigma_2$. In any case, the differential stress could be low and eventual switching of σ_1 and σ_2 might occur.

The W*NW–ESE joint set* should be related to an extensional stress field with NNE-trending σ_3 trajectories. This interpretation is compatible with the main macrostructures described in the region (Alcubierre basement normal fault, Ebro syncline, tectolineaments), which show similar strikes and have been interpreted as a result of extensional deformation.

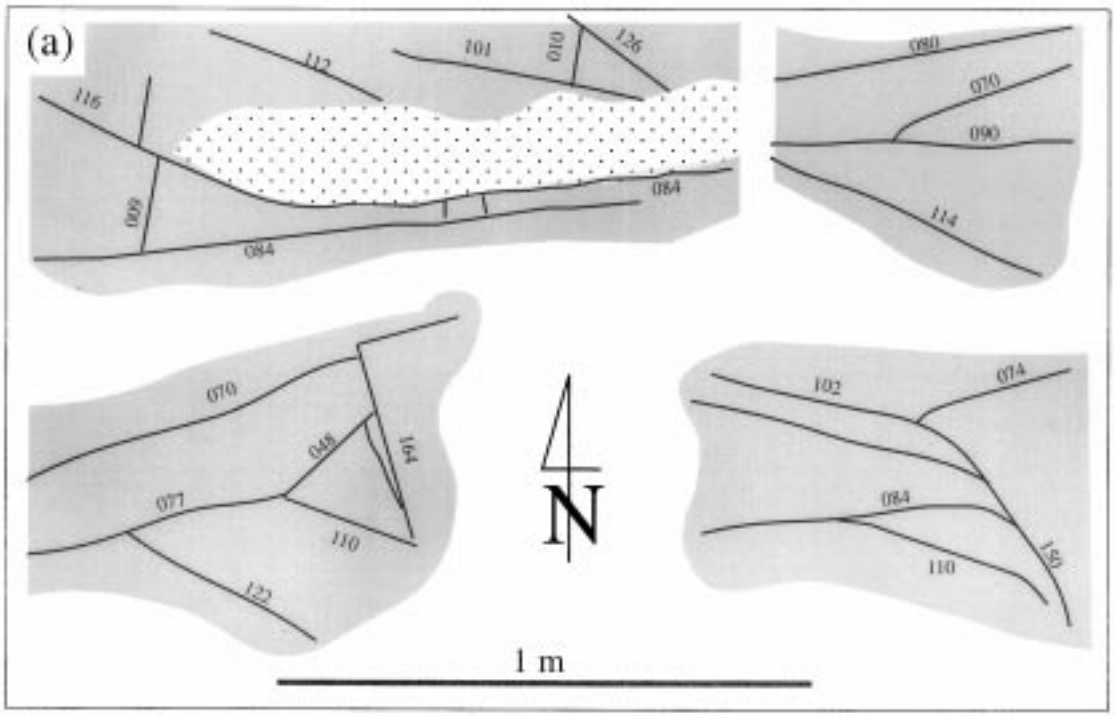
(a)
112
101
010
126
116
084
089
084
080
070
090
114
070
048
164
077
110
122
N
102
014
084
110
150
1 m

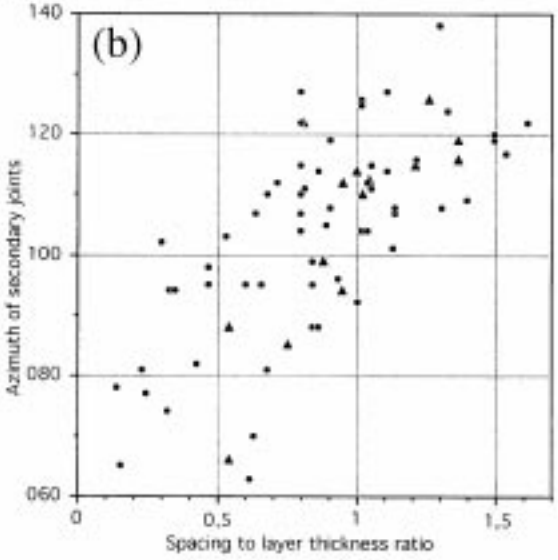
(b)
140
120
100
080
060
0
0,5
1
1,5
Azimuth of secondary joints
Spacing to layer thickness ratio

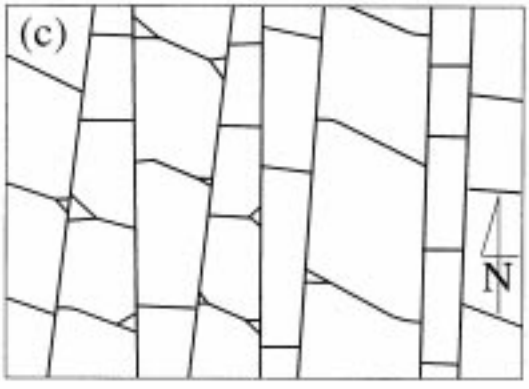
(c)
N

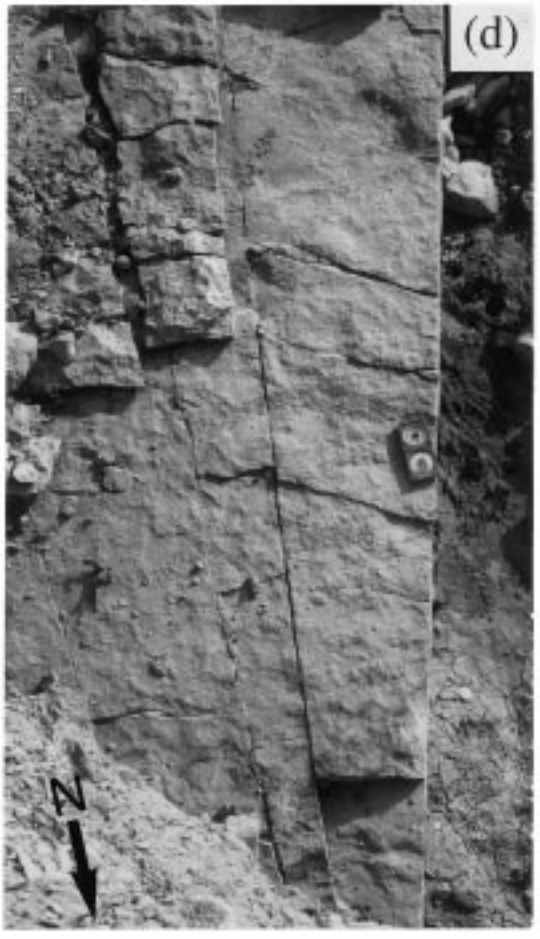
(d)
N

The former interpretation emphasises the control of joint orientation by coeval stress fields. Accordingly, both joint sets might have formed in response to joint-normal, thermoelastic and/or fluid loads (Engelder and Fischer, 1996). It depends upon their time of propagation, either during burial or uplift of the Miocene units, respectively. We will discuss this question within the geodynamic frame of the Ebro basin.

4.2. Chronology and geodynamic significance of regional stress fields

Both the N–S and the WNW–ESE genetic joint sets are found in the uppermost levels of the Miocene series (in the case of the WNW–ESE set, it is registered as "perturbed" E–W joints). This indicates that both stress fields were active after the beginning of the late Miocene. Nevertheless, since field observations indicate that the WNW–ESE to E–W set is younger than the N–S set, we can interpret that, as a general rule, the E–W extension (N–S joint set) was earlier than the NNE–SSW extension (WNW–ESE joint set).

An independent approach can be made by discussing the development of both stress fields in the context of the tectonic framework of the Ebro basin. Considering the stress field necessary to form the N–S joints and the evolution of fault development in the region during the Neogene, a stress history with three different coaxial stress ellipsoids (Arlegui, 1996; Simón et al., 1999, fig. 2) can be identified. They all show a persistent N–S trending S_{Hmax}, the transitions being achieved by switching of the principal stress axes:

Horizontal N–S trending σ_1, vertical σ_3. Some E–W striking reverse faults developed during this stage (Arlegui, 1996; Simón et al., 1999).
Horizontal N–S trending σ_1, vertical σ_2. NNW and NNE strike-slip faults and low-angle shear fractures appeared (Hancock and Engelder, 1989; Hancock, 1991; Gil and Simón, 1992; Arlegui, 1996).
Horizontal N–S trending σ_2, vertical σ_1. N–S striking normal faults developed (Gracia and Simón, 1986; Arlegui and Simón, 1997).

The evolution of this stress field is consistent with the Neogene geodynamic frame of the northeastern Iberian Peninsula, where both N–S intraplate compression and E–W to WNW–ESE active extension occurred. The first was induced by convergence between Europe, Iberia and Africa. The second is related to rifting in the eastern margin of Iberia. Both were superposed during the Neogene, the extensional component increasing as the compressional component decreased (Simón, 1986). According to regional data, the transition from a dominantly compressional to a dominantly extensional regime took place by the middle Miocene (Simón and Paricio, 1986). Nevertheless, both stress components co-existed during the Neogene within an intraplate stress field characterised by a near N–S-trending S_{Hmax} and episodic coaxial switching of σ_1 and σ_2 axes (Simón, 1989; Cortés, 1999).

N–S joints could propagate either under σ_1 or σ_2 vertical axis during the Miocene, as sedimentary infilling of the basin progressed. We believe that joint formation and propagation was controlled by fluid pore pressure. Extension induced by uplift and exhumation was not necessary because of the rifting-induced extensional component of the regional stress field. So, according to Engelder and Fischer (1996), the N–S joints formed in response to a combination of joint-normal and fluid loads.

By the late Miocene, the central Ebro basin underwent an important change in its evolution: sedimentation slackens or ceases, and large erosion surfaces develop (Soriano, 1990). This change indicates the onset of uplift related to isostatic rebound of the Pyrenean orogen, which initiated by that time and involved the Ebro foreland basin owing to the rigidity of the lithosphere (Brunet, 1986).

Flexural isostatic uplift can explain the NNE extension registered by Miocene rocks with WNW–ESE joints. The cross-section of Fig. 3 suggests that the southern boundary of the foreland basin at an early stage of its evolution was located in the study area (see sharp thinning and extinction of the lowermost Tertiary formations under the Alcubierre range). This *subsidence hinge* of the lithosphere flexure under the Pyrenean orogenic load is interpreted by us to be the *uplift hinge* during isostatic rebound. Vertical movements accommodated by WNW–ESE striking basement faults beneath the Alcubierre-Sigena ranges induced bending folds (Ebro syncline) as well as near parallel normal faults (*tectolineaments*). According to the model of Withjack et al. (1990), deformation was probably transferred over large distances by multiple local detachment levels (either lutitic beds or units) within the Tertiary series.

From this perspective, WNW striking joints could form in the same way as the tectolineaments: as a part of the fracture ensemble propagated upward from basement faults. However, it is more probable that they essentially developed as *unloading joints* in response to a thermoelastic load (Engelder, 1985; Engelder and Fischer, 1996). Flexural

Fig. 9. Geometrical relationships between N–S, E–W and WNW–ESE joint sets at the transition zone within the Sigena section (see location in Fig. 6). (a) Outcrop sketches of abutting relationships between E–W and WNW–ESE joints. (b) Plot of azimuths of secondary WNW–ESE to E–W joints versus spacing to layer thickness ratio of each pair of systematic N–S joints enclosing them. Measurements were collected in two limestone layers: Layer 1 (triangles), thickness ranging from 42 to 45 cm, FSR for N–S joints = 1.11; Layer 2 (circles), thickness ranging from 56 to 74 cm, FSR for N–S joints = 1.21. (c) Schematic diagram showing the proposed architectural model. (d) Field example of a similar joint architecture observed near Tudela (to the West of the study area, see location in Fig. 1).

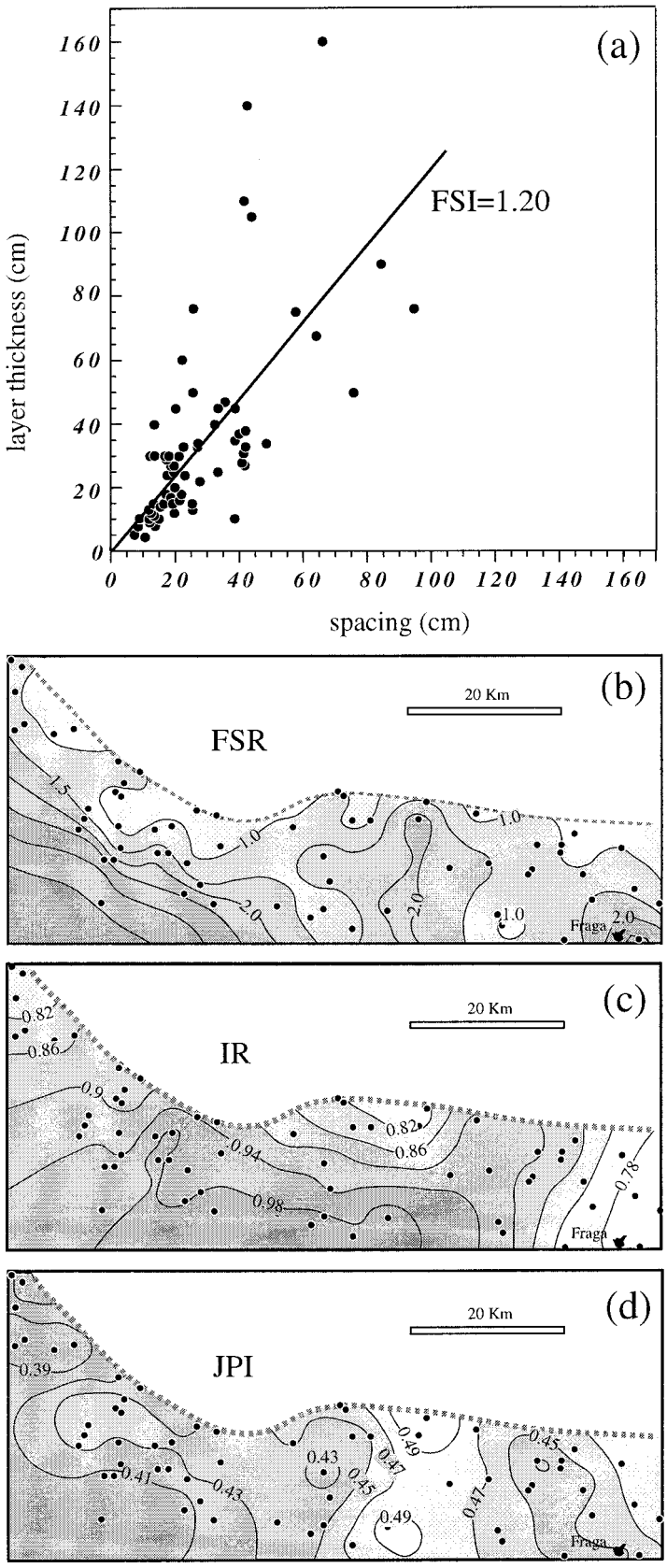

Fig. 10. (a) Layer thickness vs. joint spacing for 63 data sites. (b) Contour map of FSR values using the kriging technique. (c) The same for Joint Periodicity Index (JPI). (d) The same for Rives' Index (IR). The surveyed area is located in Fig. 6.

uplift and erosional unloading could provide the principal mechanisms for horizontal extension, given that the contemporary σ_3 trajectories are oriented orthogonal to the WNW–ESE-trending flexure axis. This hypothesis is also capable of explaining the quite homogeneous regional distribution of the WNW–ESE genetic joint set.

Our interpretations of both genetic joint sets differ in some aspects from those proposed in previous works. Turner and Hancock (1990) interpreted WNW striking joints in the northern fringe of the Ebro basin as related to basement flexure induced by thrust loading. This genetic mechanism should not be ruled out for joints observed in lower Miocene deposits near the Pyrenean front. Nevertheless, it is not adequate for WNW–ESE to E–W secondary joints found in upper Miocene beds of the Sigena range, which are not coeval with basin subsidence. According to Turner and Hancock's work, Hancock and Engelder (1989) and Hancock (1991) considered the N–S set (their *NNW striking joints*) as neotectonic, since they believed that these joints were younger than the WNW–ESE regional joint set. Nevertheless, we have shown that the N–S joints are older than the WNW–ESE ones in the central Ebro basin, contradicting Hancock and Engelder's interpretation.

4.3. Interpretation for spatial distribution of N–S joints using a numerical approach

The inhomogeneous spatial distribution of the N–S and WNW–ESE joints may be related to a number of factors which determine either horizontal or vertical variations of effective stress (overburden and pore-fluid pressure, distribution of stress sources, stress perturbations). Remember that the inhomogeneity basically concerns the N–S set, in which both horizontal and vertical variations of joint saturation have been found. Moreover, these variations are responsible for the qualitative difference between the joint pattern in the northern sector (primary WNW–ESE striking joints) and the southern sector (N–S primary joints, E–W secondary joints).

Why did the intraplate stress field produce N–S joints all over the upper Oligocene to upper Miocene deposits of the southern sector, but not in the northern one? In our opinion, this distribution might be the consequence of two factors: (1) moderate stress magnitudes, close to the critical values needed for tensional failure in Miocene limestones of the Ebro basin; (2) differences in fluid pore pressures from the southern to the northern sector, determined by the depth of the free water table. This idea is based upon the results of some calculations of theoretical effective stress and stress intensity made for different hypotheses of N–S compression, E–W rifting extension and depth of the water table. Though this presentation does not constitute a detailed mathematical model, this numerical approach does explain differences of several hundred metres in depth attained by the N–S joints in the southern sector with respect to the northern one (Fig. 11).

Our analysis is based on Price's model of stress superposition in elastic materials (Price, 1966, pp. 69–71). According to this approach, the values of the principal effective stresses are given by:

vertical axis: $\sigma_z = \rho g h - P_f$

N–S horizontal axis: $\sigma_y = (\rho g h)\nu/(1-\nu) + C_y + E_x\nu - P_f$

E–W horizontal axis: $\sigma_x = (\rho g h)\nu/(1-\nu) + C_y\nu + E_x - P_f$,

where ρ is mean density (in our case, 2.5 g/cm^3), h is depth, P_f is fluid pore pressure, ν is Poisson's ratio, C_y is N–S intraplate compression and E_x is E–W rifting-induced tension.

We have estimated a Poisson's ratio $\nu = 0.22$ for chalky limestones near the surface, and it has been supposed to vary with depth as described by Price (1966), p. 70). That variation has been included into the model using a simplified equation: $\nu = 1/(4.5 - h)$, where h is expressed in km.

Pore-fluid pressure determined by the presence of a free water table is interpreted to have varied with Miocene palaeogeography: lacustrine environment in the innermost basin and southwards sloping fluvial system coming from the Pyrenees (Quirantes, 1978; Riba et al., 1983). So, the water table should be situated over the surface in the southern sector, and should become deeper with respect to the land surface to the north (Fig. 12).

Stress conditions for jointing have been analysed using two alternative criteria. First, we considered tensional failure to occur when the absolute value of σ_3 is greater than the tensile strength of Miocene limestones. The latter was measured in the laboratory (Gil and Simón, 1992), showing an average value of 65 bars. Second, we have utilised the *fracture toughness* or *critical stress intensity factor* (K_{IC}) that must be attained close to cracks for them to propagate as Mode I fractures. *Stress intensity* (K_I) for an embedded crack oriented normal to the layer is

$$K_I = \sigma'(\pi a)^{1/2},$$

where σ' is the effective tensile stress parallel to the layer and a is the half crack length (Tada et al., 1973). Engelder (1987) pointed out that fractures in sedimentary rocks usually propagate from flaws larger than microcracks. We have used crack length $2a = 1$ cm, which is the same value utilised by Lemiszki et al. (1994) for stress intensity calculations in limestone. Finally, as we have no direct measurement of fracture toughness in "our" rocks, we decided to use values published by Schmidt and Huddle (1977) (in Lemiszki et al., 1994, fig. 4) for Indiana limestone. The following linear regression results were chosen to represent the rate of change of fracture toughness with confining stress σ_c:

$$K_{IC} = 0.45 + 0.053\sigma_c,$$

where σ_c is expressed in MPa and K_{IC} is expressed in

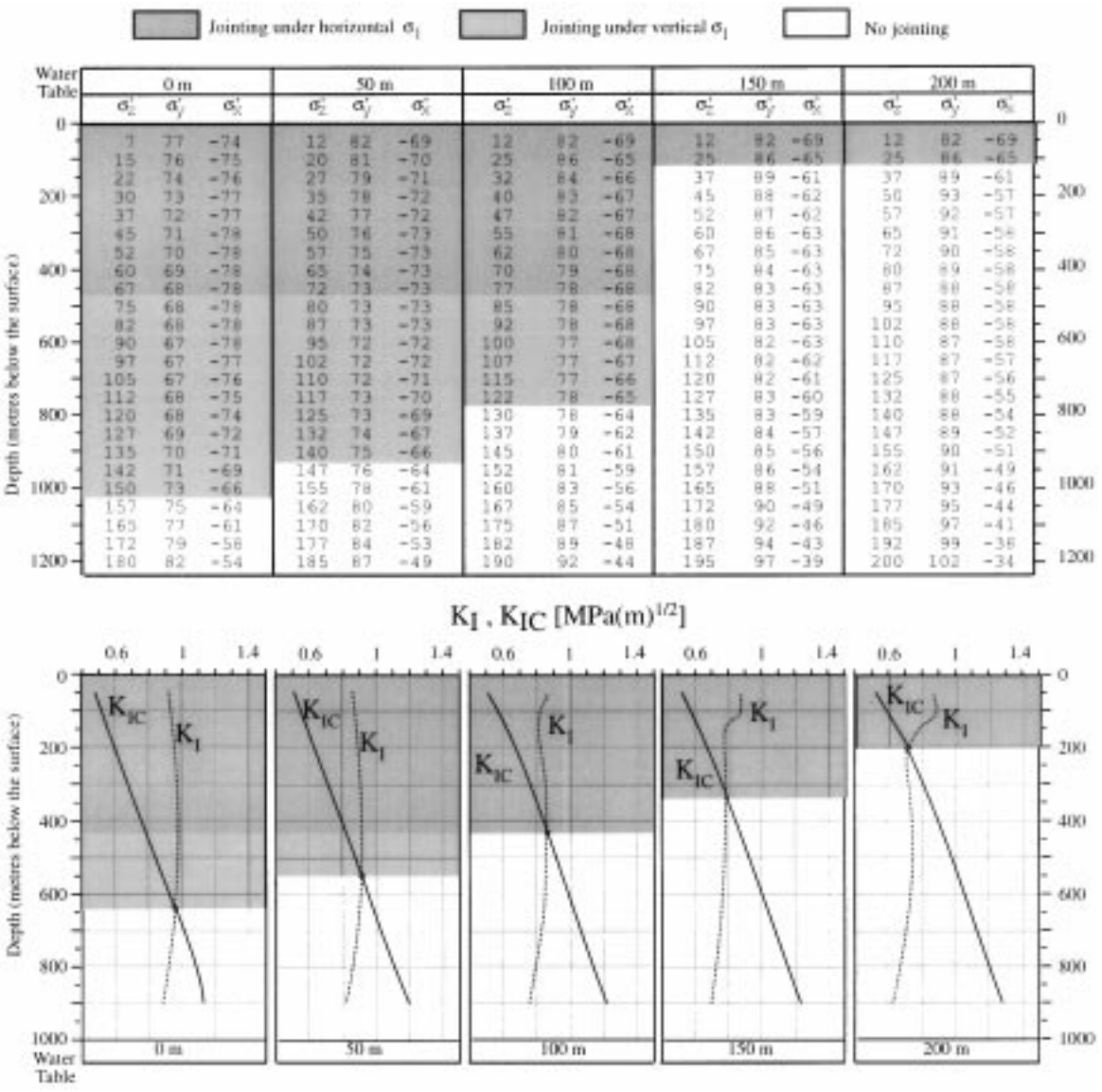

Fig. 11. Numerical simulation of effective stress field compatible with the spatial distribution of N–S joints. Further explanation in text.

MPa(m)$^{1/2}$. According to the former conditions, propagation of Mode I fractures will occur when

$$K_I \geq K_{IC} \quad \text{or} \quad \left|\sigma'_x(0.005\pi)^{1/2}\right| \geq |0.45 + 0.053\sigma'_z|,$$

σ'_x and σ'_z being expressed in MPa.

Fig. 11 shows an example of numerical simulation of effective stress compatible with the observed distribution of N–S joints. Arbitrary values of remote N–S compression $C_y = 100$ bars and E–W tension $E_x = -95$ bars have been superposed onto the lithostatic overburden to illustrate the effects of these tectonic stress components. The principal effective stresses σ'_z (vertical), σ'_y (maximum horizontal stress) and σ'_x (minimum horizontal stress) have been calculated (in bars) at different depths under given pore-fluid pressure conditions according to the water table. Five water table depths are considered from south to the north, at 0, 50, 100, 150 and 200 m below the land surface, respectively. Using tensile strength (Fig. 11a), the resulting stress distribution allows development of tensional joints up to a depth of about 1000 m in the southern sector and only 100 m in the northern one. Using fracture toughness (Fig. 11b), Mode I joints would attain a depth of 650 m in the southern sector and 200 m in the northern one.

Similar results can be obtained using a range of values for the tectonic stress components: C_y (100–300 bars, approximately) and E_x (about −100 bars). Combinations of larger absolute values either give rise to the development of strike-slip faults instead of joints or do not produce a significant variation of the depth attained by joints. Smaller values do not allow brittle failure to occur.

In any case, given the lack of true constraints for the

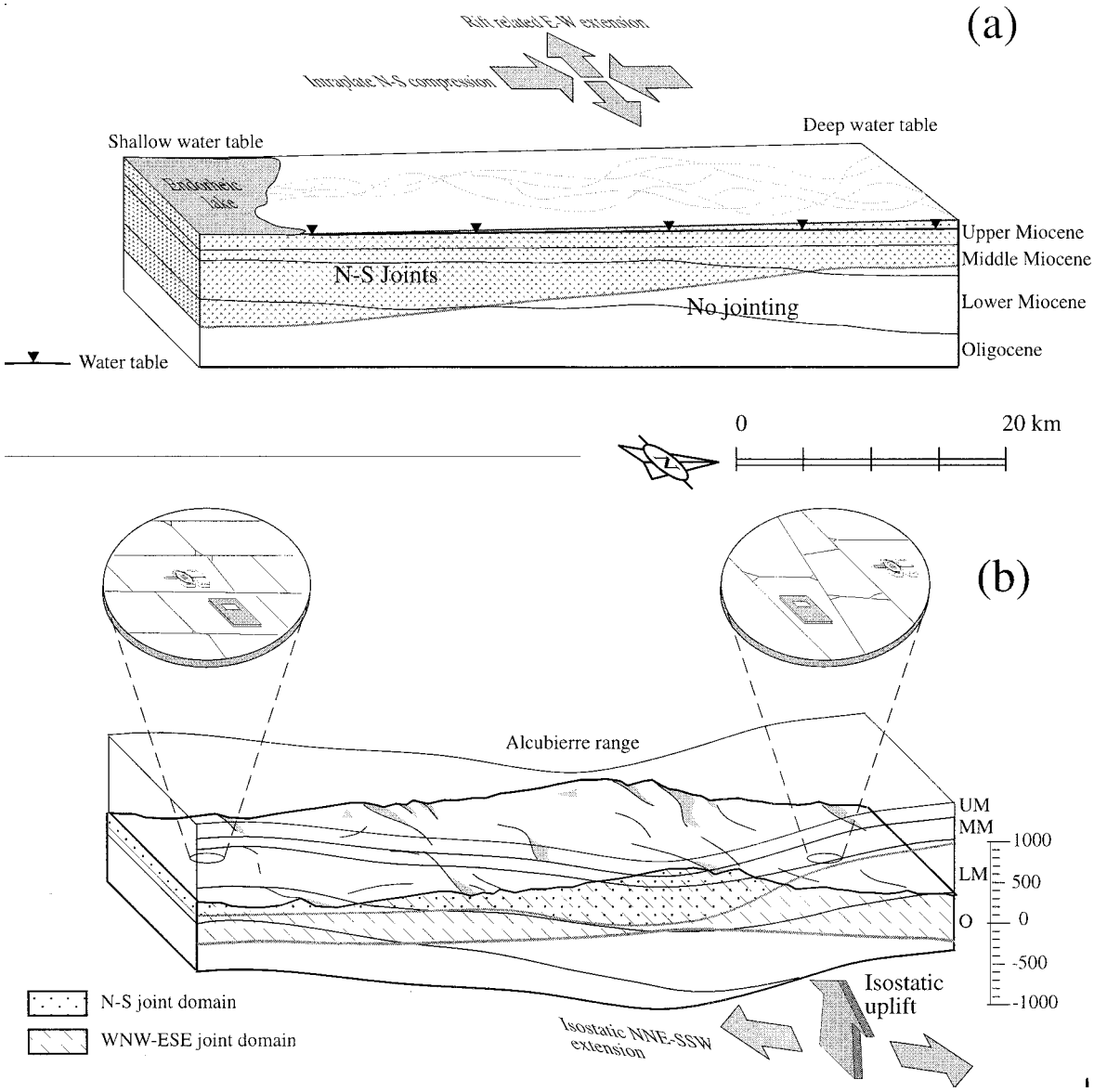

Fig. 12. Schematic model of the relationships between regional scale deformation, stress directions and joint development. (a) Period of basin subsidence (early–late Miocene). (b) Period of isostatic rebound (after late Miocene). The model has been drawn taking into account the macrostructure described in Figs. 2 and 3 and the results of mathematical simulation. Further explanation in text.

various stress component magnitudes, only the qualitative features of the model should be retained for consideration. Our approach does not describe the precise conditions in which jointing did occur. Our purpose is just to show how adequate combinations of tectonic stress, lithostatic overburden and fluid pore pressure may account for the observed change in the vertical distribution of N–S striking joints with changing horizontal position.

5. Conclusions

Joints in the Ebro basin constitute a penetrative structure which allows us to reconstruct Neogene paleostress fields and their evolution. The results are consistent with the geodynamic framework of the northeastern Iberian Peninsula.

Three regional joint sets have been defined with azimuths close to N–S, WNW–ESE and E–W, respectively. N–S and WNW–ESE joints are persistent parallel joints that are older than other fractures in their host rocks, whereas E–W joints are younger cross joints abutting N–S ones.

The spatial distribution of joint sets is not homogeneous. The N–S set and the associated E–W cross joint set predominate in the central and southern sectors, whereas the WNW–ESE systematic set appears in the northern one. A well-defined boundary along the northern side of the Alcubierre-Sigena ranges separates both joint domains.

Geometry of this boundary indicates that the N–S joint domain is not only *southward*, but also locally *upward*, with respect to the WNW–ESE domain. Within the narrow transition zone where the three joint sets are found together, cross-cut relationships indicate that the WNW–ESE and E–W joint sets are coeval and younger than the N–S ones.

N–S joints are interpreted to develop during basin infilling in response to joint-normal and fluid loads with S_{Hmax} oriented near N–S (Fig. 12a), which evolved from strike-slip to extensional regime by switching the σ_1 and σ_2 axes. This stress field resulted from superposition of N–S intra-plate compression and E–W to WNW–ESE rifting-induced tension. The pervasive occurrence of the N–S joint set in the southern sector and their virtual restriction to the uppermost levels in the northern one may be attributed to two factors: (1) moderate magnitudes of external forces, satisfying certain combinations of N–S compression and E–W tension; (2) differences in pore-fluid pressure determined by depth of the water table, which increased northward from the lacustrine environment of the innermost basin (south) to into the subsurface under the fluvial system coming from the Pyrenees.

WNW–ESE to E–W joints are formed by flexural uplift and thermoelastic loading during exhumation related to isostatic rebound (Fig. 12b). In the northern sector, they propagated as systematic joints in the absence of the N–S set; their orientation was controlled by preferred NNE–SSW extension orthogonal to the flexural axis. In the southern sector, they propagated as secondary E–W joints owing to perturbation of stress trajectories by pre-existing N–S joints.

Acknowledgements

We thank R.J. Lisle who kindly reviewed a preliminary version of the manuscript. We also thank the Editor, W. Dunne, and the two referees, T. Engelder and W. Narr, for their critical and useful comments. L. Arlegui holds a post-doctoral fellowship financed by the FPI program of the Spanish Government.

References

Arenas, C., 1993. Sedimentología y Paleogeografía del Terciario del Margen Pirenaico y Sector Central de la Cuenca del Ebro (Zona Aragonesa Occidental). Ph.D. thesis, Universidad de Zaragoza.

Arenas, C., Pardo, G., 1994. Estratigrafía del margen septentrional aragonés de la Cuenca del Ebro (Sector Uncastillo-Bolea). II Congreso del G.E.T., Jaca, 19–21 September 1994, pp. 31–34.

Arlegui, L.E., 1992. Métodos de investigación aplicables a las diaclasas. Ejemplos de los Monegros, Cuenca del Ebro. III Congreso Geológico de España y VIII Congreso Latinoamericano de Geología, Actas, 1, Salamanca, June 1992, pp. 259–264.

Arlegui, L.E., 1996. Diaclasas, fallas y campo de esfuerzos en el sector central de la Cuenca del Ebro. Ph.D. thesis, University of Zaragoza.

Arlegui, L.E., Hancock, P.L., 1991. Interpreting joint systems from their architecture: examples from the Ebro Basin, Spain. 22nd Annual Meeting of the Tectonic Studies Group, Edinburgh.

Arlegui, L.E., Simón, J.L., 1993. El sistema de diaclasas N–S en el sector central de la Cuenca del Ebro. Relación con el campo de esfuerzos neógeno. Revista de la Sociedad Geológica de España 6 (1-2), 115–122.

Arlegui, L.E., Simón, J.L., Soriano, M.A., 1994. Un sistema regional de fracturas NW–SE en el centro de la Cuenca del Ebro. II Congreso del Grupo Español del Terciario, Jaca, 19–21 September. Comunicaciones, pp. 39–43.

Arlegui, L.E., Simón, J.L., 1997. El sistema de fallas normales de las Bárdenas (Navarra) en el marco del campo de esfuerzos neógeno. In: Calvo, J.P., Morales, J. (Eds.), Avances en el conocimiento del Terciario Ibérico. Museo Nacional de Ciencias Naturales, Madrid, pp. 29–33.

Arlegui, L.E., Soriano, M.A., 1998. Characterising lineaments from satellite images and field studies in the central Ebro basin (NE Spain). International Journal of Remote Sensing 19 (16), 3169–3185.

Bergerat, F., Angelier, J., Bouroz, C., 1991. L'analyse des diaclases dans le Plateau du Colorado (USA): une clé pour la reconstruction des paléo-contraintes. Comptes Rendues Academie Sciences Paris, Série II 312, 309–316.

Bevan, T.G., Hancock, P.L., 1986. A late cenozoic regional mesofracture system in southern England and northern France. Journal of the Geological Society of London 143, 355–362.

Brunet, M.F., 1986. The influence of the evolution of the Pyrenees on adjacent basins. Tectonophysics 129, 345–354.

Cabrera, L., 1983. Estratigrafía y sedimentología de las formaciones lacustres del tránsito Oligoceno–Mioceno del SE de la Cuenca del Ebro. Ph.D. thesis, Universidad de Barcelona.

Caputo, R., 1995. Evolution of orthogonal sets of coeval extension joints. Terra Nova 7 (5), 479–490.

Cobbold, P.R., 1979. Origin of periodicity; saturation or propagation? Description and origin of spatial periodicity in tectonic structures; report on a tectonic studies group conference. Journal of Structural Geology 1, 96.

Cortés, A., 1999. Evolución tectónica reciente de la Cordillera Ibérica, Cuenca del Ebro y Pirineo Centro-Occidental. Ph.D. thesis, University of Zaragoza.

Davis, G.H., 1984. Structural Geology of Rocks and Regions. John Wiley, New York.

Desegaulx, P., Moretti, I., 1988. Subsidence history of the Ebro basin. Journal of Geodynamics 10, 9–24.

Dunne, W.M., Hancock, P.L., 1994. Palaeostress analysis of small-scale brittle structures. In: Hancock, P.L. (Ed.), Continental Deformation. Pergamon Press, Oxford, pp. 101–121.

Dyer, R., 1988. Using joint interactions to estimate paleostress ratios. Journal of Structural Geology 10 (7), 685–699.

ECORS-Pyrenees Team, 1988. The ECORS deep reflection seismic survey across the Pyrenees. Nature 331, 508–511.

Engelder, T., 1985. Loading paths to joint propagation during a tectonic cycle: an example from the Appalachian Plateau, USA. Journal of Structural Geology 7 (3/4), 459–476.

Engelder, T., 1987. Joint and shear fractures in rock. In: Atkinson, B.K. (Ed.), Fracture Mechanics of Rock. Academic Press Geology Series, Harcourt Brace Jovanovitch, pp. 27–69.

Engelder, T., Fischer, M.P., 1996. Loading configurations and driving mechanisms for joints based on the Griffith energy-balance concept. Tectonophysics 256, 253–277.

Engelder, T., Geiser, P., 1980. On the use of regional joint sets as trajectories of paleostress fields during the development of the Appalachian Plateau, New York. Journal of Geophysical Research 85 (B11), 6319–6341.

Engelder, T., Gross, M.R., 1993. Curving cross joints and the lithospheric stress field in eastern North America. Geology 21, 817–820.

Gil, I., Simón, J.L., 1992. Aproximación al cálculo de los valores absolutos

de paleoesfuerzos compresivos en el Mioceno inferior de Tudela (Navarra). Geogaceta 11, 31–34.

Goldstein, A., Marshak, S., 1988. Analysis of fracture array geometry. In: Marshak, S., Mitra, G. (Eds.), Basic Methods of Structural Geology. Prentice Hall, Englewood Cliffs, NJ, pp. 249–267.

Gracia, F.J., Simón, J.L., 1986. El campo de fallas miocenas de la Bardena Negra (Provs. de Navarra y Zaragoza). Boletín Geológico y Minero 97, 693–703.

Griffith, A.A., 1920. The phenomena of rupture and flow in solids. Philosophical Transactions of the Royal Society of London A221, 163–198.

Griffith, A.A., 1924. The theory of rupture. In: Biezeno, C.B., Burgers, J.M. (Eds.), Proceedings of the First International Congress on Applied Mechanics, Waltman, Delft, pp. 54–63.

Gross, M.R., 1993. The origin and spacing of cross joints: examples from the Monterey Formation, Santa Barbara Coastline, California. Journal of Structural Geology 15 (6), 737–751.

Gross, M.R., Fischer, M.P., Engelder, T, Greenfield, R.J., 1995. Factors controlling joint spacing in interbedded sedimentary rocks: integrating numerical models with field observations from the Monterey Formation, USA. Geological Society Special Publication No. 92, pp. 215–233.

Hancock, P.L., 1985. Brittle microtectonics: principles and practice. Journal of Structural Geology 7, 437–457.

Hancock, P.L., 1991. Determining contemporary stress directions from neotectonic joint systems. Philosophical Transactions of the Royal Society of London A337, 29–40.

Hancock, P.L., Engelder, T., 1989. Neotectonic joints. Geological Society of America Bulletin 101, 1197–1208.

Hobbs, D.W., 1967. The formation of tension joints in sedimentary rocks: an explanation. Geological Magazine 104, 550–556.

Hodgson, R.A., 1961. Classification of structures on joint surfaces. American Journal of Science 259, 493–502.

Holts, T.B., Foote, G.R., 1981. Joint orientation in Devonian rocks in the Northern portion of the lower Peninsula of Michigan. Geological Society of America Bulletin 92, 85–93.

IGME, 1990. Documentos sobre la geología del subsuelo de España. Tomo VI (cuenca del Ebro-Pirineo). IGME, Madrid.

ITGE, 1995a. Mapa Geológico de España, escala 1:50,000, Hoja 356 (Lanaja). ITGE, Madrid.

ITGE, 1995b. Mapa Geológico de España, escala 1:50,000, Hoja 385 (Castejón de Monegros). ITGE, Madrid.

Kulander, B.R., Barton, C.C., Dean, S.L., 1979. The application of fractography to core and outcrop fracture investigations. US Department of Energy, Morgantown Energy Technology Center, MET/SP-79/3, 174 p.

Lanaja, J.M., 1987. Contribución de la exploración petrolífera al conocimiento de la geología de España. IGME, Madrid.

Lemiszki, P.J., Landes, J.D., Hatcher Jr, R.D., 1994. Controls on hinge-parallel extension fracturing in single-layer tangential-longitudinal strain folds. Journal of Geophysical Research 99 (B11), 22027–22041.

Liesa, C.L., 2000. Fracturación y campos de esfuerzos compresivos alpinos en la Cordillera Ibérica y el NE peninsular. Ph.D. thesis, Universidad de Zaragoza.

Liotta, D., 1990. La distribuzione dei joints nel bacino di Santa Barbara (Valdarno superiore): indicazioni sulla tectonica neogenica. Boll. Soc. Geol. It. 109, 437–444.

Matheron, G., 1971. The theory of regionalised variables and its applications. Cah. Cent. Morph. Math. 5.

Muñoz, J.A., 1992. Evolution of a continental collision belt: ECORS-Pyrenees crustal balanced cross-section. In: McClay, K.R. (Ed.), Thrust Tectonics. Chapman & Hall, London, pp. 235–246.

Narr, W., Suppe, J., 1991. Joint spacing in sedimentary rocks. Journal of Structural Geology 13 (9), 1037–1048.

Pollard, D.D., Aydin, A., 1988. Progress in understanding jointing over the past century. Geological Society of America Bulletin 100, 1181–1204.

Pollard, D.D., Segall, P., Delaney, P.T., 1982. Formation and interpretation of dilatant echelon cracks. Geological Society of America Bulletin 93, 1291–1302.

Price, N.J., 1966. Fold and Joint Development in Brittle and Semi-brittle Rocks. Pergamon Press, Oxford.

Price, N.J., Cosgrove, J.W., 1990. Analysis of Geological Structures. Cambridge University Press, Cambridge.

Puigdefàbregas, C., Souquet, P., 1986. Tectonosedimentary cycles and depositional sequences of the Mesozoic and Tertiary of the Pyrenees. Tectonophysics 129, 173–203.

Quirantes, J., 1978. Estudio sedimentológico y estratigráfico del Terciario Continental de los Monegros. Publicación 681 de la Institución Fernando el Católico (CSIC) de la Diputación de Zaragoza, 207 pp.

Rawnsley, K.D., Rives, T., Petit, J.-P., Hencher, S.R., Lumsdem, A.C., 1992. Joint development in perturbed stress fields near faults. Journal of Structural Geology 14 (8/9), 939–951.

Riba, O., Reguant, S., Villena, J., 1983. Ensayo de síntesis estratigráfica y evolutiva de la cuenca terciaria del Ebro. Libro Jubilar J.M. Ríos: Geología de España, IGME.

Rives, T., 1992. Mecanismes de formation des diaclases dnas les roches sedimentaires. Approche expérimentale et comparaison avec quelques exemples naturels. Ph.D. thesis, Université des Sciences et Techniques de Languedoc, Montpellier II.

Rives, T., Razack, M., Petit, J.P., Rawnsley, K.D., 1992. Joint spacing: analogue and numerical simulations. Journal of Structural Geology 14 (8/9), 925–937.

Roure, F., Choukroune, P., Berastegui, X., Muñoz, J.A., Villien, A., Matheron, P., Bareyt, M., Séguret, M., Camara, P., Déramond, J., 1989. ECORS deep seismic data and balanced cross-sections: geometric constrainst to trace the evolution of the Pyrenees. Tectonics 8, 41–50.

Ruf, J.C., Rust, K.A., Engelder, T., 1998. Investigating the effect of mechanical discontinuities on joint spacing. Rock Deformation; the Logan Volume. Tectonophysics 295 (1–2), 245–257.

Schmidt, R.A., Huddle, C.W., 1977. Effect of confining pressure on fracture toughness of Indiana limestone. International Journal of Rock Mechanics and Mining Sciences. 14 (5–6), 289–293.

Simón, J.L., 1986. Analysis of a gradual change in stress regime (example from the eastern Iberian Chain, Spain). Tectonophysics 124, 37–53.

Simón, J.L., 1989. Late Cenozoic stress field and fracturing in the Iberian Chain and Ebro Basin (Spain). Journal of Structural Geology 11(3), 285–294.

Simón, J.L., Paricio, J., 1986. Sobre la compresión neógena en la Cordillera Ibérica. Estudios Geológicos 44, 271–283.

Simón, J.L., Serón, F.J., Casas, A.M., 1988. Stress deflection and fracture development in a multidirectional extension regime. Mathematical and experimental approach with field examples. Annales Tectonicae II (1), 21–32.

Simón, J.L., Arlegui, L.E., Liesa, C.L., Maestro, A., 1999. Stress perturbations registered by jointing near strike-slip, normal and reverse faults. Examples from the Ebro Basin (Spain). Journal of Geophysical Research 104 (B7), 15141–15153.

Soriano, M. A. 1990. Geomorfología del sector centromeridional de la Depresión del Ebro. Institución Fernando el Católico, publicación 1231.

Tada, H., Paris, P.C., Irwin, G.R., 1973. The Stress Analysis of Cracks Handbook. Del Research Corporation, Hellertown, PA.

Turner, J.P., Hancock, P.L, 1990. Thrust systems of the southwest Pyrenees and their control over basin subsidence. Geological Magazine 127 (5), 383–392.

Watson, G.S., 1971. Trend-surface analysis. Math. Geol. 3, 215–226.

Wise, D., McCrory, T.A., 1982. A new method of fracture analysis: azimuth versus traverse distance plots. Geological Society of America Bulletin 93, 889–897.

Withjack, M.O., Olson, J., Peterson, E., 1990. Experimental models of extensional forced folds. American Association of Petroleum Geologists Bulletin 74, 1038–1054.

Wu, H., Pollard, D.D., 1995. An experimental study of the relationships between joint spacing and layer thickness. Journal of Structural Geology 17 (6), 887–905.